Available online at www.sciencedirect.com

SciVerse ScienceDirect

Ceramics International 38 (2012) 5821–5825

CERAMICS INTERNATIONAL

www.elsevier.com/locate/ceramint

Effect of chlorine ion concentration on morphology and optical properties of Cl-doped ZnO nanostructures

Ramin Yousefi [a,*], Farid Jamali-Sheini [b]

[a] Department of Physics, Masjed-Soleiman Branch, Islamic Azad University (I.A.U), Masjed-Soleiman, Iran
[b] Department of Physics, Ahwaz Branch, Islamic Azad University, Ahwaz, Iran

Received 14 December 2011; received in revised form 9 April 2012; accepted 9 April 2012
Available online 16 April 2012

Abstract

Effect of Cl^{-1} concentration on morphology and optical properties of Cl-doped ZnO nanostructures was studied. The Cl-doped ZnO nanostructures and undoped ZnO microstructures were grown on Si(1 1 1) substrates using a physical vapor deposition method. The ZnO nanostructures have been doped with different concentrations of chlorine. The Cl-doped ZnO nanostructures with 6% atom Cl, showed a nanodisk morphology with a hexagonal shape, while the Cl-doped ZnO nanostructures with 9% atom Cl, exhibited a stacked nanoplate morphology with smaller thickness in comparison to the Cl-doped ZnO nanodisks. In addition, with increasing Cl content to 13%, morphology of the products changed to more stacked nanoplates with nanoflakes morphology. X-ray diffraction results clearly showed a hexagonal structure for the all samples. Raman spectroscopy results showed a strong crystalline quality for the undoped ZnO microdisks and Cl-doped ZnO nanodisks; while these results indicated a weak crystalline quality for the Cl-doped ZnO nanoplates and nanoflakes. Photoluminescence (PL) studies also confirmed the Raman results and it exhibited a lower optical property for the Cl-doped ZnO nanoplates and nanoflakes in comparison to the undoped ZnO microdisks and Cl-doped ZnO nanodisks. Furthermore, the UV peak of the Cl-doped ZnO nanostructures was blue-shifted with respect to that of the undoped ZnO.

Keywords: Cl-doped ZnO nanodisks; Cl-doped ZnO nanoplates; Cl-doped ZnO nanoflakes; Undoped ZnO microdisks; Optical properties

1. Introduction

ZnO has a direct band-gap of 3.37 eV and a high exciton binding energy of 60 meV, which is greater than the thermal energy at room temperature. In addition, ZnO has shown splendid and abundant nanostructure configurations that a material can form. As is well known, the impurity-doping of semiconductors with selective elements greatly affects their basic physical properties such as their electrical, optical, and magnetic properties, which are crucial for their practical application. The literature shows that much attention has been paid to cationic doping in ZnO nanostructures. We have also employed cationic doping for ZnO nanostructures including the use of Mg, Al, and In [1–5]. On the other hand, less attention has been paid to the anionic doping effect on the morphology and optical properties of ZnO nanostructures. However, we studied the optical properties of S-doped ZnO nanobelts in our previous work [6]. We also performed a comparative study between optical properties of S and Sn-doped ZnO nanobelts [7]. We observed that when S was used for anionic doping, it affected the visible emission of the PL spectrum, while when Sn was used for cationic doping; it affected the UV emission of the PL spectrum.

It is known, halogen elements can also be used as substitution elements for O as anionic doping. Furthermore, these elements reduce the oxygen adsorption on surfaces [8]. Several groups have studied the optical properties of Cl-doped ZnO nanostructures with different morphologies [8–13], but effect of Cl content on optical properties of Cl-doped ZnO nanostructures has been paid less attention.

According to these reasons, in this work, Cl-doped ZnO nanostructures were grown on silicon substrates using a thermal evaporation method. The effects of using chlorine as an anionic dopant and content of chlorine on the morphology and optical properties of the ZnO nanostructures were investigated using

* Corresponding author. Tel.: +98 9166224993; fax: +98 6813330093.
E-mail address: yousefi.ramin@gmail.com (R. Yousefi).

0272-8842/$36.00
http://dx.doi.org/10.1016/j.ceramint.2012.04.030

field emission scanning electron microscope, X-ray diffractometer (XRD), Raman and photoluminescence (PL) spectrometers.

2. Experimental

The growth of Cl-doped ZnO nanostructures was performed in a horizontal furnace. ZnO films growth process was already described elsewhere [4,5]. A mixture of zinc oxide powder (99.99%) and commercial graphite powder at a 1:1 weight ratio was used as the precursor material for the ZnO, and NaCl powder (99.99%) was used for the precursor material of Cl (Mol_{ZnO}/Mol_{NaCl} = 10:2, 10:3, 10:4). The precursor material for the ZnO was placed at the closed end of the smaller quartz tube and a Si(1 1 1) substrate was placed downstream of the precursor materials. The precursor materials were heated to 950 °C and the temperature of the substrate was maintained at 550 °C during the growth process for the Cl-doped ZnO nanostructures. High purity N_2 gas was fed at about 100 sccm into the furnace at one end, while the other end was connected to a rotary pump. The growth process was allowed to proceed for 1 h. A vacuum of 6 Torr was maintained inside the tube furnace during the deposition of the nanostructures. In this manner, three sets of Cl-doped ZnO nanostructures made with different chlorine content. Undoped ZnO were also grown under the same conditions using a catalyst-free substrate.

The crystal structure and morphology of the products were investigated using a field emission scanning electron microscope (FESEM, Quanta 200 F) and an X-ray diffractometer (XRD, Siemens D5000). The elemental contents of the products were investigated using energy dispersive X-ray analysis (EDX, Quanta 200 F). Room temperature photoluminescence and Raman (Jobin Yvon Horiba HR 800 UV) spectroscopies were employed to study the optical properties and crystallinity of the Cl-doped ZnO nanodisks and undoped ZnO disks. A He–Cd laser with a wavelength of 325 nm and an Ar ion laser with an emission wavelength of 514.5 nm were used for the PL and Raman measurements, respectively.

3. Results and discussion

Fig. 1(a) shows an FESEM image of the undoped ZnO. As can be seen, the morphology of the undoped ZnO is microdisks. The microdisks have a wide distribution of diagonals, from

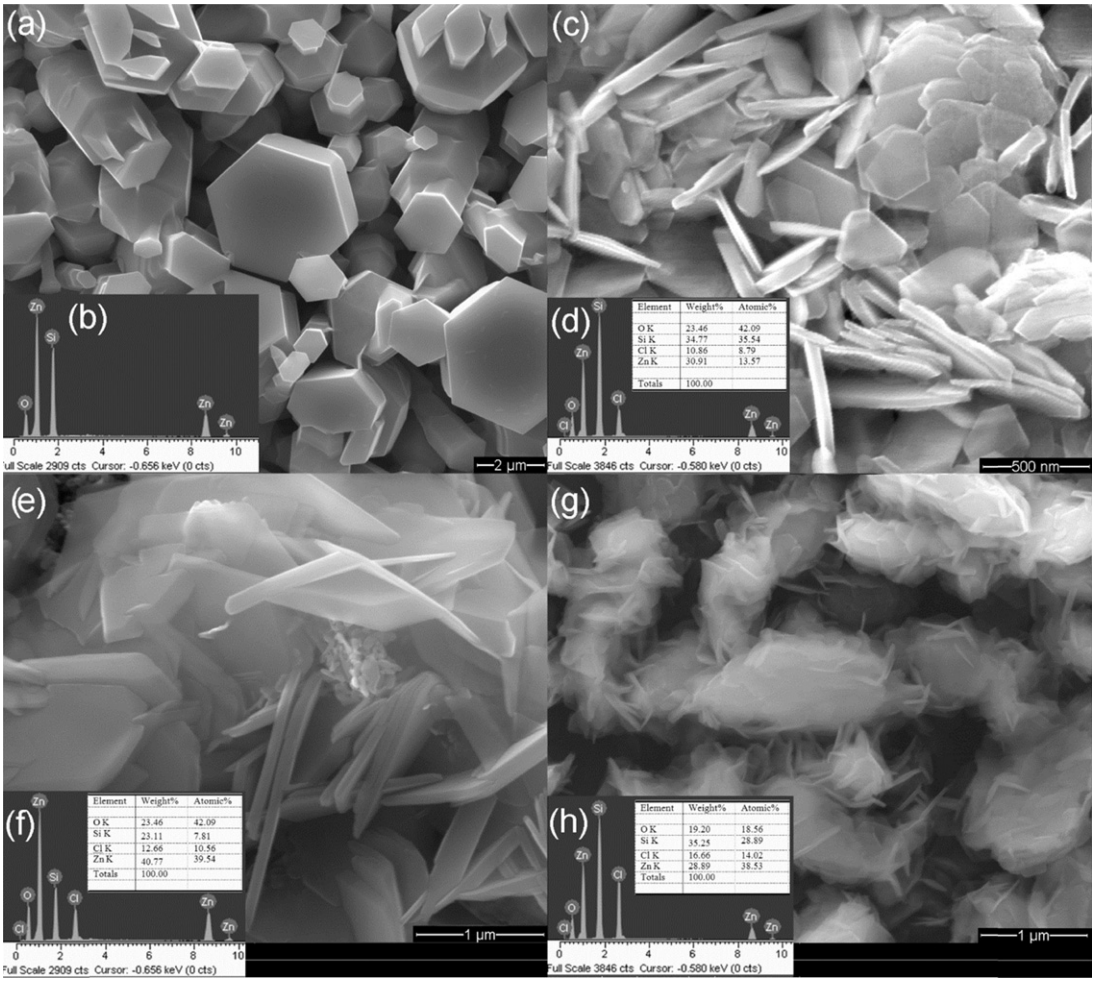

Fig. 1. (a) FESEM image of the undoped ZnO microdisks. (b) EDX spectrum of the ZnO microdisks. (c) FESEM image of the Cl-doped ZnO nanodisks. (d) EDX spectrum of the Cl-doped ZnO nanodisks. (e) FESEM image of the Cl-doped ZnO nanoplates. (f) EDX spectrum of the Cl-doped ZnO nanoplates. (g) FESEM image of the Cl-doped ZnO nanoflakes. (h) EDX spectrum of the Cl-doped ZnO nanoflakes.

800 nm to 4 μm, with a thickness about 1 μm and a perfect hexagonal geometry. The orientation of the microdisks growth is preferentially along the direction of the *c*-axis ([0 0 0 1]), because the *c*-axis is perpendicular to the hexagonal plane. In addition, because no catalyst was used in the growth of the ZnO microdisks in this study, the growth occurs via a vapor–solid (VS) mechanism. The absence of any detectable catalyst and impurity at the ZnO microdisks surface supports this statement. Fig. 1(b) shows an EDX spectrum of undoped ZnO microdisks. The spectrum indicates the microdisks are pure ZnO; however, a signal from the Si substrate is also detected. Fig. 1(c) shows an FESEM image of the Cl-doped ZnO nanodisks. As can also be clearly seen, the Cl-doped ZnO nanodisks have a hexagonal shape, but the distribution of the diagonal of the Cl-doped ZnO nanodisks is very narrow (250–300 nm). In addition, the thickness of the Cl-doped ZnO nanodisks is on the order of several tens of nanometers. The average thickness of Cl-doped ZnO nanodisks is about 85 nm. Although many of the nanodisks are stacked together, most of them lie on the substrate in a horizontal position, while some stand up vertically. Fig. 1(d) shows an EDX spectrum of the Cl-doped ZnO nanodisks. The EDX spectrum shows about a 6% (atomic) content for the Cl element and no peaks are detected from other materials such as Na. Fig. 1(e) shows an FESEM image of the second set of the Cl-doped ZnO nanostructures. The FESEM image reveals that the morphology of nanostructures is nanoplates for the second set. The average thickness of Cl-doped ZnO nanoplates is about 60 nm. It can be clearly seen, the nanoplates stacked together completely, and most of them stand up vertically. Fig. 1(f) shows an EDX spectrum of the Cl-doped ZnO nanoplates. The EDX spectrum indicates about a 9% (atomic) content for the Cl element and no peaks are also detected from other materials such as Na. An FESEM image of the third set of the Cl-doped ZnO nanostructures is shown in Fig. 1(g). It can be seen that the morphology of the third set is nanoflakes. The nanoflakes are very thin and average thickness of them is about 48 nm. The EDX spectrum of these nanostructures is shown in Fig. 1(h). The EDX spectrum shows about a 13% (atomic) content for the Cl element and no peaks are also detected from other materials such as Na. According to the FESEM images, the morphology of the Cl-doped ZnO nanostructures is affected by increasing Cl content in the products. In fact, with increasing Cl content, the nanostructures become thinner.

Fig. 2 shows XRD patterns of the undoped ZnO microdisks and Cl-doped ZnO nanostructures. The XRD patterns in Fig. 2 agree with the standard card of bulk ZnO with a hexagonal structure (JCPDS No. 800075). No peaks from Zn, Cl, or other impurities are visible. The dominant peak of (0 0 2) for the undoped ZnO microdisks and Cl-doped ZnO nanodisks indicates that in most of the ZnO disks, the [0 0 0 1] direction is perpendicular to the substrate. On the other hand, the XRD patterns of the Cl-doped ZnO nanoplates and nanoflakes show (1 0 1) peak as dominant peak with two peaks with the same intensity ((1 0 0) and (0 0 2) peaks) that could be due to random direction of the plates on the Si substrate in these samples. The ionic radius of the substitute Cl^{1-} (rCl^{1-} = 0.18 nm) is bigger

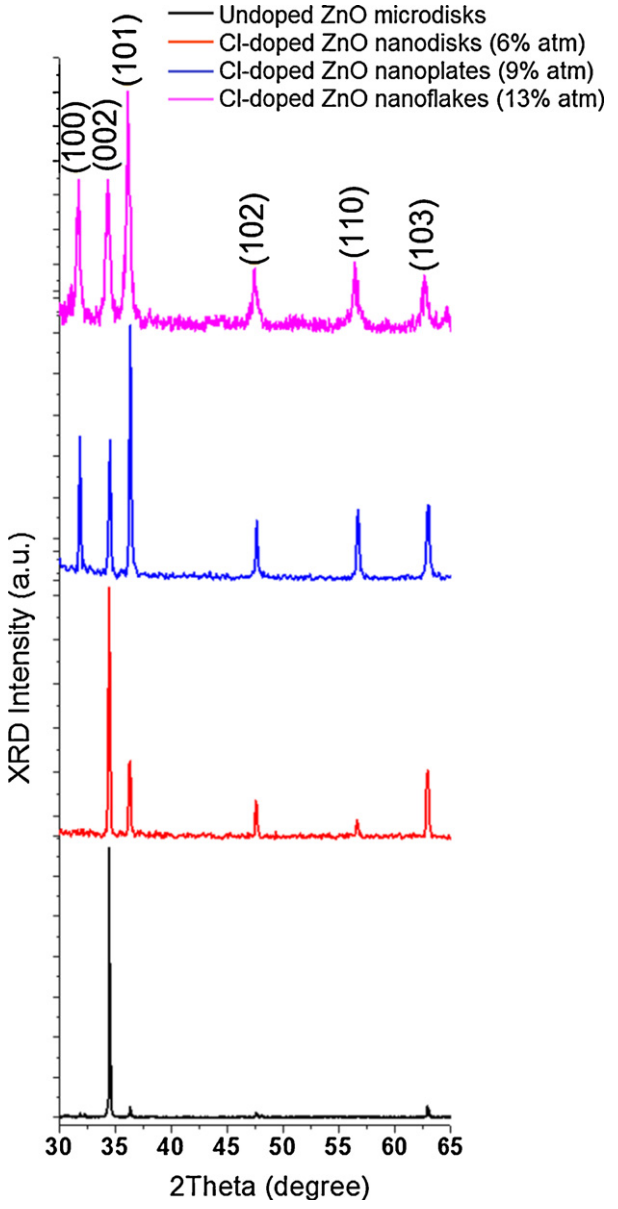

Fig. 2. XRD patterns of the undoped ZnO microdisks and the Cl-doped ZnO nanostructures. The patterns show hexagonal structures for the all samples.

than that of O^{2-} (rO^{2-} = 0.14 nm). Thus, doping with Cl causes a slight shift in the (0 0 2) peaks toward lower diffraction angles. This result provides indirect evidence that chlorine is incorporated into the crystal structure, causing the ZnO crystal lattice to expand.

The growth process of the undoped ZnO microdisks can be explained by the following reactions:

$$ZnO(s) + C(s) \rightarrow Zn(g) + CO(g) \quad (1)$$

$$ZnO(s) + CO(g) \rightarrow Zn(g) + CO_2(g) \quad (2)$$

$$Zn(g) + CO(g) \rightarrow ZnO(\text{microdisks}) \quad (3)$$

In fact, graphite was introduced into the raw materials to reduce the oxides into metals, as shown in reaction (1). Moreover, the sublimed Zn atoms are carried downstream by

the diffusion process, and in the lower-temperature region, Zn atoms condense and form liquid clusters, which tend to deposit uniformly onto the silicon substrate. The liquid droplets quickly solidify on the substrate in the deposition temperature zone. From a surface-energy point of view, the lowest energy facets for Zn are $\{0\,0\,0\,1\}$, and then $\{1\,0\,\bar{1}\,0\}$ and $\{2\,\bar{1}\,\bar{1}\,0\}$. Thus, faceted, single crystalline Zn hexagonal disks tend to form, which are enclosed by $\{0\,0\,0\,1\}$ top and bottom surfaces and $\{1\,0\,\bar{1}\,0\}$ side surfaces. Considering the lower local growth temperature, the residual oxygen in the growth chamber is likely to oxidize the surface of the Zn disks, but the degree to which the disks are oxidized depends on the local temperature and amount of oxygen in chamber. On the basis of the information that we gathered, a growth process for the hexagonal disks can be proposed. If the (0 0 0 2) facet of the crystallized ZnO is constantly kept clean and the newly incoming droplets can constantly wet and cover the entire condensed (0 0 0 2) facet, the ZnO disks with a geometrical shape of hexagonal projections can be obtained [14]. In our experimental conditions, the mobility of the Zn atoms in the vapor was high enough to form flat (0 0 0 2) surfaces which prevented the accumulation of incoming atoms or molecules [15]. The smooth surface of the disk, as shown in the SEM image in Fig. 1(a), provides the evidence for this assumption. However, one question arises here: Why were thin nanodisks obtained from the sample that was doped with Cl? According to the following reactions

$$\mathrm{NaCl(s)} \rightarrow \mathrm{NaCl(g)} \tag{4}$$

$$\mathrm{Zn(g)} + x\mathrm{CO(g)} + 2x\mathrm{NaCl(g)} + 1/2\mathrm{O_2} \rightarrow \mathrm{ZnO_{(1-2x)}Cl_{2x}(nanodisks)} + x\mathrm{Na_2CO_3} \tag{5}$$

some of the oxygen in the chamber serves to generate $x\mathrm{Na_2CO_3}$ and Cl substitutes for oxygen during the oxidation of the Zn. Therefore, the lower oxidation of the Zn droplets during the growth of the Cl-doped ZnO disks causes the Cl-doped ZnO disks to be smaller than the undoped disks. Thus, we infer that the Cl^{1-} may serve as a surface-passivating agent in the reaction system. Because the ZnO crystal is a polar material in nature with a (0 0 0 1) surface terminated by Zn^{2+} ions, the opposite ions (Cl^{1-}) would be adsorbed by charge compensation. The adsorption of Cl^{1-} on the Zn^{2+} terminated faces resulted in the redistribution of the surface energy and the growth rates of the different facets changed. The growth process took place at the interface of the Zn terminated facets by the combination of Cl^{1-}. Accordingly, the intrinsic growth of ZnO along the [0 0 0 1] direction is substantially suppressed forming the ZnO nanodisks. Therefore, we believe that Cl^{1-} ions act as a passivation agent by charge compensation and slow the growth of ZnO along the [0 0 0 1] direction, leading to the formation of Cl-doped ZnO hexagonal nanodisks. In fact, the dopants effect on the formation of ZnO nanodisks is caused by the polar property of ZnO in the [0 0 0 1] direction. In addition, by increasing the chlorine concentration in the reactor ZnO nanostructures grow with more poor oxygen. Therefore, more poor oxygen during the growth process of Cl-doped ZnO causes that morphology of ZnO nanodisks changes to nanoplates and nanoflakes. In fact, Cl concentration is a significant factor to obtain different morphology for the Cl-doped ZnO nanostructures.

Raman spectroscopy is an effective technique for estimating the crystallinity of materials. According to the group theory, single crystalline ZnO belongs to the C^4_{6V} space group, with two formula units per primitive cell and eight sets of optical phonon modes at the Γ point of the Brillouin zone, classified as $A_1 + E_1 + 2E_2$ modes (Raman active), $2B_1$ modes (Raman silent) and $A_1 + E_1$ modes (infrared active). The E_1 and A_1 modes are two polar modes and are split into transverse optical (TO), and longitudinal optical (LO) branches. The Raman spectra for the undoped ZnO microdisks and Cl-doped ZnO nanostructures are presented in Fig. 3. As shown in Fig. 3, the Raman spectra show sharp, strong, and dominant peaks at 437 cm^{-1} and 438.1 cm^{-1} for the undoped ZnO microdisks and Cl-doped ZnO nanodisks, respectively, corresponding to the E_2(high) mode of the Raman active mode, a characteristic peak for the wurtzite hexagonal phase of ZnO. On the other hand, this peak appears with a weak intensity at 439 cm^{-1} for the Cl-doped ZnO nanoplates and at 439.6 cm^{-1} for the Cl-doped ZnO nanoflakes. In fact, a weak E_2(high) peak of the Raman spectra of Cl-doped ZnO nanostructures with higher Cl concentration, shows that crystallinity of these nanostructures decreases due to more Cl ions in ZnO structures. Appearing a strong peak at 579 cm^{-1} of the Raman spectra for both samples with nanoplates and nanoflakes morphology, is a good evidence for this claim that Cl^{-1} can decrease crystallinity of ZnO nanostructures. Because, the peak at 579 cm^{-1} belongs to E_1(LO), that is associated with impurities and formation of defects such as oxygen vacancies [16]. Therefore, the appearance a strong E_1(LO) peak for the both samples indicates a lower crystalline quality and higher oxygen vacancy for them. In addition, it can be seen that, the E_2(high) peak of Cl-doped ZnO nanostructures is blue shifted in comparison to the E_2(high) peak of the undoped ZnO microdisks. This result is consistent with the observed lattice expansion from the XRD measurements.

A PL study is a powerful method for investigating the effects of impurity doping on optical properties of ZnO nanostructures, because doped ZnO nanostructures are expected to have different optical properties in comparison with undoped ZnO. Fig. 4 shows the room temperature PL spectra of the undoped

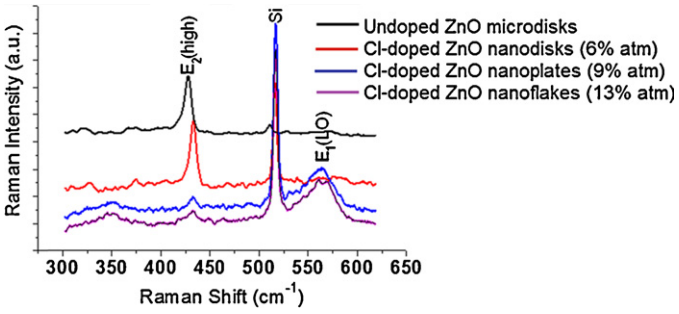

Fig. 3. Raman spectra of the undoped ZnO microdisks and the Cl-doped ZnO nanostructures.

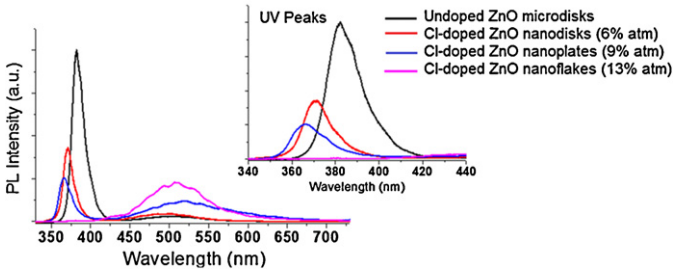

Fig. 4. PL spectra of the undoped ZnO microdisks and the Cl-doped ZnO nanostructures.

ZnO microdisks and Cl-doped ZnO nanostructures. It can be seen, a significant different between the spectra. The PL spectra of undoped ZnO microdisks and Cl-doped ZnO nanodisks show a strong peak in the ultraviolet (UV) region (370.2–382 nm) and a negligible green emission (deep-level emission (DLE)) peaks in the visible region at around 480 nm. On the other hand, the PL spectrum of the Cl-doped ZnO nanoplates shows the UV and DLE peak with the same intensity approximately, and the PL spectrum of the Cl-doped ZnO nanoflakes shows no detectable UV peak and a strong DLE peak. In addition, compared with the undoped ZnO microdisks, the PL spectrum of the Cl-doped ZnO nanostructures shows an obvious blueshift in the UV emission. This blueshift in the UV emission is believed to be a result of the Burstein–Moss effect because of the Cl doping in the ZnO nanostructures. The stronger intensity of the DLE, the more singly ionized oxygen vacancies there are. Therefore, Fig. 4 shows that the Cl-doped ZnO nanoplates and nanoflakes have very high concentrations of oxygen vacancies. Since chlorine has a larger ionic radius than oxygen, the incorporation of Cl into the ZnO lattice will introduce lattice distortion. This effect influences the energy band structure of the ZnO nanostructures doped with chlorine, and as a result, new defects such as oxygen vacancies can be introduced by the new band structure deformation. Based on this reason, the DLE peaks are dominant peaks in the PL result of the as-grown Cl-doped ZnO nanostructures with higher concentration of Cl. Undetectable UV peak in the Cl-doped ZnO nanoflakes could be also attributed to more substitution of O with Cl. Such optical behavior of ZnO nanostructures has been observed in our previous work that the ZnO nanostructures have been doped by sulfur [6]. When, we compare our previous results from cationic dopants with anionic dopants, it can be understood that cationic dopants affect the UV part of the PL results, while anionic dopants affect the visible part of the PL results. In fact, these results can help us to fabricate ZnO nanostructures for any laser and light sources in the close future.

4. Conclusion

The physical vapor deposition method was used to grow Cl-doped ZnO nanostructures with different concentration of Cl and undoped ZnO microstructures. It was observed that, the Cl^{1-} played an important role to obtain ZnO nanostructures with different morphologies. The PL and Raman results showed that crystallinity and optical properties of Cl-doped ZnO nanostructures decreased with increasing Cl concentration. In addition, the UV peaks of the PL spectra were blueshifted for the Cl-doped ZnO nanostructures in comparison with the undoped ZnO microdisks. This indicated that the Cl^{1-} doping induced the Burestin–Moss effect and band gap increasing in the ZnO nanodisks.

Acknowledgment

R. Yousefi gratefully acknowledges the financial support by the Masjed-Soleiman Branch, Islamic Azad University (I.A.U), Iran. In addition, F. Jamali-Sheini acknowledges the financial support by the Islamic Azad University (I.A.U), Ahwaz Branch.

References

[1] R. Yousefi, M.R. Muhamad, A.K. Zak, Thin Solid Films 518 (2010) 5971.
[2] R. Yousefi, B. Kamaluddin, M. Ghoranneviss, F. Hajakbari, Applied Surface Science 255 (2009) 6985.
[3] R. Yousefi, B. Kamaluddin, Applied Surface Science 256 (2009) 329.
[4] R. Yousefi, M.R. Muhamad, Journal of Solid State Chemistry 183 (2010) 1733.
[5] R. Yousefi, F.J. Sheini, M.R. Muhamad, M.A. More, Solid State Sciences 12 (2010) 1088.
[6] R. Yousefi, B. Kamaluddin, Solid State Sciences 12 (2010) 252.
[7] R. Yousefi, B. Kamaluddin, Applied Surface Science 255 (2009) 9376.
[8] J.B. Cui, Y.C. Soo, T.P. Chen, Journal of Physical Chemistry C 112 (2008) 4475.
[9] Z. Tao, X. Yu, X. Fei, J. Liu, G. Yang, Y. Zhao, S. Yang, L. Yang, Optical Materials 31 (2008) 1.
[10] Z. Tao, X. Yu, X. Fei, J. Liu, L. Yang, S. Yang, Materials Letters 62 (2008) 1187.
[11] E. Chikoidze, M. Modreanu, V. Sallet, O. Gorochov, P. Galtier, Physica Status Solidi (a) 205 (2008) 1575.
[12] J. Elias, R. Tena-Zaera, C. Lévy-Clément, Journal of Physical Chemistry C 112 (2008) 5736.
[13] F.J. Sheini, Ceramics International 38 (2012) 3649.
[14] Z.R. Dai, Z.W. Pan, Z.L. Wang, Advanced Functional Materials 13 (2002) 9.
[15] Z.R. Dai, Z.W. Pan, Z.L. Wang, Journal of Physical Chemistry B 106 (2002) 902.
[16] Y.J. Xing, Z.H. Xi, Z.Q. Xue, X.D. Zhang, J.H. Song, R.M. Wang, J. Xu, Y. Song, S.L. Zhang, D.P. Yu, Applied Physics Letters 83 (2003) 1689.